2007 American WJTA Conference and Expo

August 19-21, 2007 ● Houston, Texas

Paper

DYNAMIC ANALYSIS OF THE SPATIAL-TEMPORAL BEHAVIOUR OF THE CUTTING FRONT IN ABRASIVE WATERJET CUTTING

A. Henning, E. Westkämper,

Fraunhofer Institute for Production Engineering and Automation

Nobelstr. 12, 70569 Stuttgart, Germany

henning@ipa.fhg.de

ABSTRACT

Abrasive water jets have become a recent tool in mechanical machining. With its great advantages of geometrical and material flexibility and its ability of cutting hard-to-machine materials the technology is more and more spreading among industries. Due to the very complex and highly dynamic process most approaches to modelling of the process focus at the analysis of the stationary result.

In this paper new approaches to analysis of the cutting front are elaborated. With the utilisation of a high speed optical measurement system the dynamic behaviour of the cutting front is analysed. New insights about the particle-material interaction could be gained by evaluation the shape of the very cutting front and its spatial and temporal development. With this a better understanding of the participating processes new approaches to modelling the abrasive waterjet can be initiated resulting in possible optimisation of the overall outcome regarding surface quality and cutting performance.

Organized and Sponsored by the WaterJet Technology Association

1 INTRODUCTION

Abrasive waterjets have been established in many fields of industrial production. With wider distribution of this promising technology it becomes more and more important to generate better understanding of the very processes and their dynamic behaviour. In early promising approaches many authors (e.g. Hashish, 1988) found high speed imaging suitable to gain information about the phenomenal behaviour of the cutting process. Recent studies (Henning, 2006) of the quantitative erosion patterns lead to new insights of the relevant processes. With the utilisation of a high speed optical measurement system the dynamic behaviour of the cutting front was analyzed and new insights about the particle-material interaction could be gained by evaluation the shape of the very cutting front. With this a better understanding of the participating processes new approaches to modeling the abrasive waterjet could be initiated resulting in possible optimization of the overall outcome regarding surface quality and cutting performance.

2 GEOMETRY OF THE CUTTING FRONT

2.1 Macroskopic cutting front

The cutting process at abrasive waterjet cutting is caused by multiple impacts from particles that are accelerated by a high speed waterjet in an abrasive mixing chamber and focussing nozzle. Those highly kinetic particles directly impact on the workpiece forming the primary cutting zone (Figure 1). After this first impact the particles can have consecutive impacts in the secondary cutting zone. Here a cutting front with a very significant shape is formed.

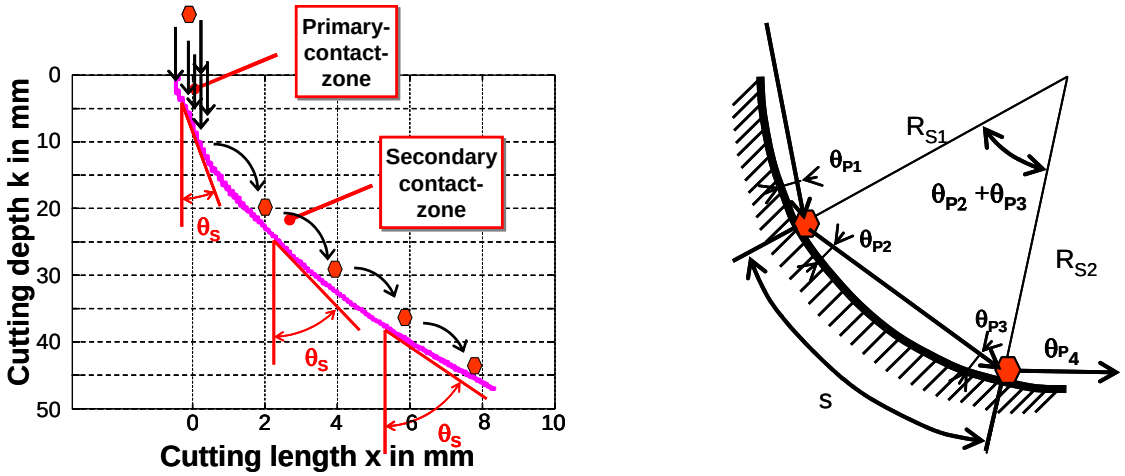

Figure 1: Appearance of the cutting front with associated impact situation

Material removal at the cutting front mostly takes place in experimentally observed erosion waves at steps that move down the cutting front (compare Figure 5). Between those disturbances

of the shape of the cutting front it always returns to its significant shape with particles moving along at high velocity and high kinetic energy without significant volume removal in feed direction. Through this locally reduced federate more sidewall contacts of the particles occur which leads to widening of the cutting front and thus striation marks at the cutting edge along the significant shape.

At this stage the particles have multiple impacts at the cutting edge without causing major erosion wear. In Figure 1 the geometry of a contact situation at a curved surface is shown. The exiting conditions of one impact would always determine the entrance condition of the next impact. Velocity and rotation of the particle does not change between the impacts. Therefore the exit condition of one impact would be exactly the entrance condition of the next. If one would assume that the curvature remains constant between two contacts this is also true for the exit and impact angle ($\theta_{P3}= \theta_{P2}$). With this the curvature κ which is the change of contour angle θ_s over the arclength s becomes

$$\kappa(z) = \frac{\theta_{P2} + \theta_{P3}}{\Delta s}$$
$$\kappa(z) = 2\theta_{P2} / \Delta s \qquad (1)$$

In previously described experimental studies the limit cycle of the cutting appeared as parabolic shape. This shape shows a decreasing curvature. With the geometric analysis in Figure 2 significant changes from entrance to exit angle one impacting situation are to be expected. Due to the multitude of particles in the process with varying properties this can only be a general or quantitative view of the process. Still at this limit cycle the process comes to a stage where the particles maintain most of their kinetic energy and cause only little erosion at the very cutting front. Therefore the cutting front remains at this position resulting in increased erosion at the side walls of the cutting edge. This erosion can be observed as striation marks at the cutting edge after completion of the cutting process. For analysis of the relevant processes it is necessary to have a detailed view on the very impact situation.

2.2 Geometry at step formation

The macroscopic cutting front shows a very stable behaviour. As high speed photography has shown microscopic effects play an important role in the abrasive cutting process. Steps are identified to appear at the cutting front interrupting the steady behaviour of the front. When analyzing the local geometry at the step (Figure 2c) it is appearent that even at small steps large deviations in contour angle and curvature occur (Figure 2a and Figure 2b). The local contour angle θ_A takes on a maximum at the top of the step. The curvature takes on positive values at the top part of the step, changes its sign at the very step and takes on negative values. When combining those two graphs into a phase diagram of contour angle over curvature (Figure 2d) a circle like trajectory can be observed. The circle takes has two zero-points of curvature. The top of the step can be observed at the upper most part of the circle. The bottom part of the circle shows at the minimum point of the local angle the macroscopic contour angle θ_S.

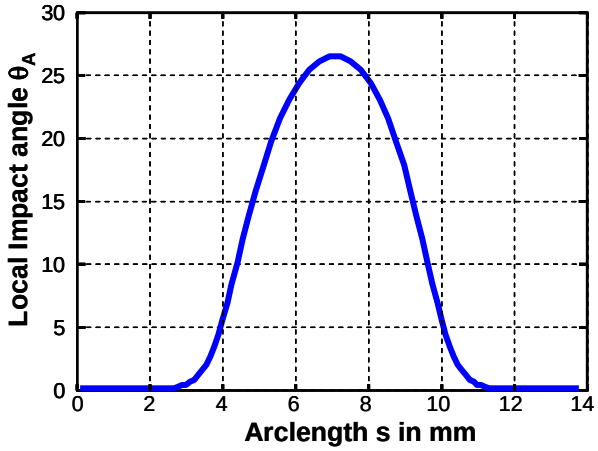

a) Local contour angle θ_A at step formation

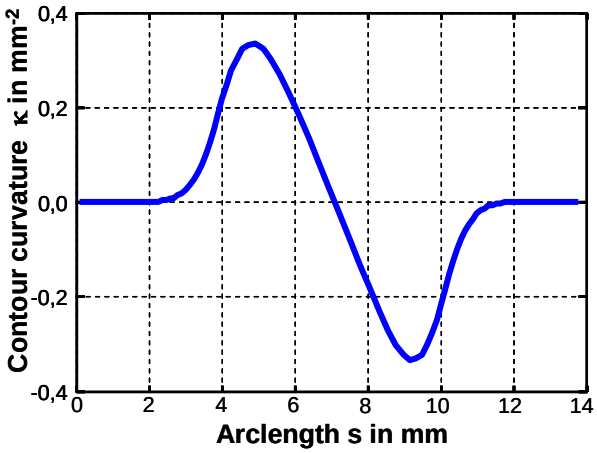

b) Local curvature κ at step formation

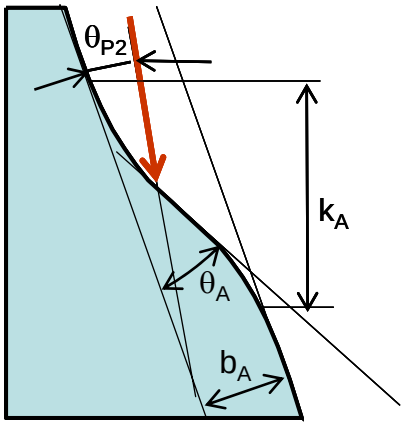

c) Schematic view of a step

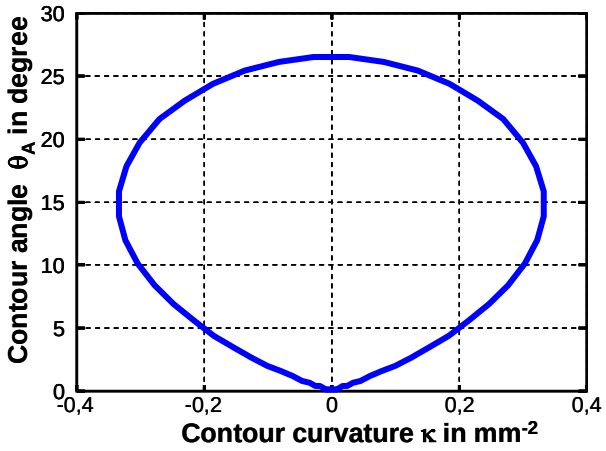

d) Phase diagramm of step formation

Figure 2: Geometric Factors at step formation

3 EXPERIMENTAL ANALYSIS

At normal cutting operation the cutting front cannot be observed since it is subject to continous changes. Still for analysis of the very processes it is important to gain information about the geometry and the spatio-temporal development of the cutting front. For the analysis transparent probes of acrylic glas (PMMA) were used to gain understanding of the local erosion processes. In Figure 3 an experimental setup with a high speed measuring device is pictured. As shown in the right picture at this setup the very cutting front can be identified very well. With this setup the cutting front could be observed at 519 frames per second and an original spatial resolution of 50µm.

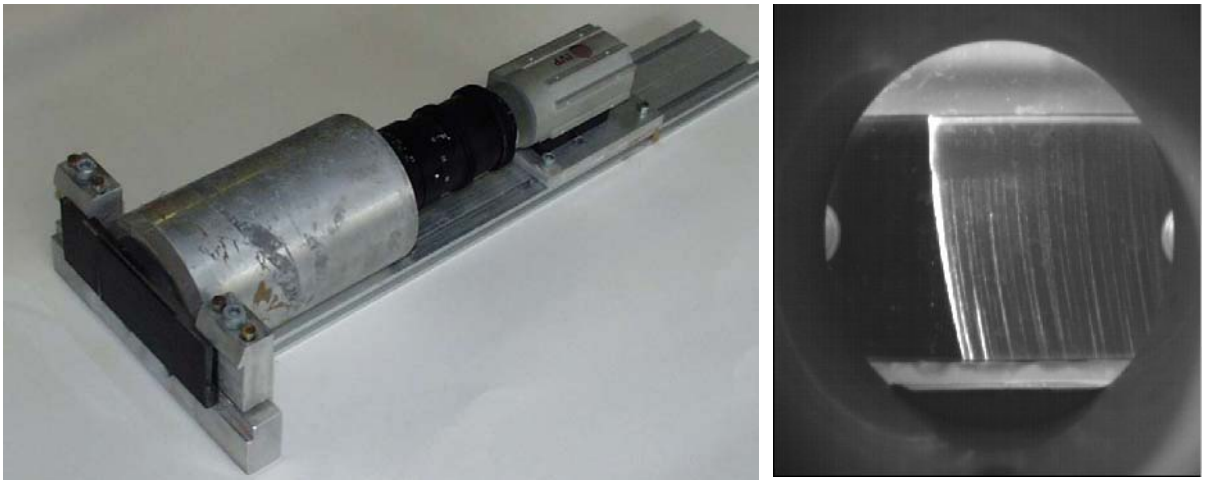

Figure 3: Experimental setup for high speed analysis

In Figure 4 a selection of the observed cutting fronts (appr. 35 per second) is shown. At this figure zones higher and lower density can be observed. As the time increment of the cutting fronts is constant higher density in this picture can be associated with lower erosion rate. Already here discontinuous processes can be visualized. Still the general shape of the cutting front always returns to its stable limit cycle (indicated as red lines in Figure 4).

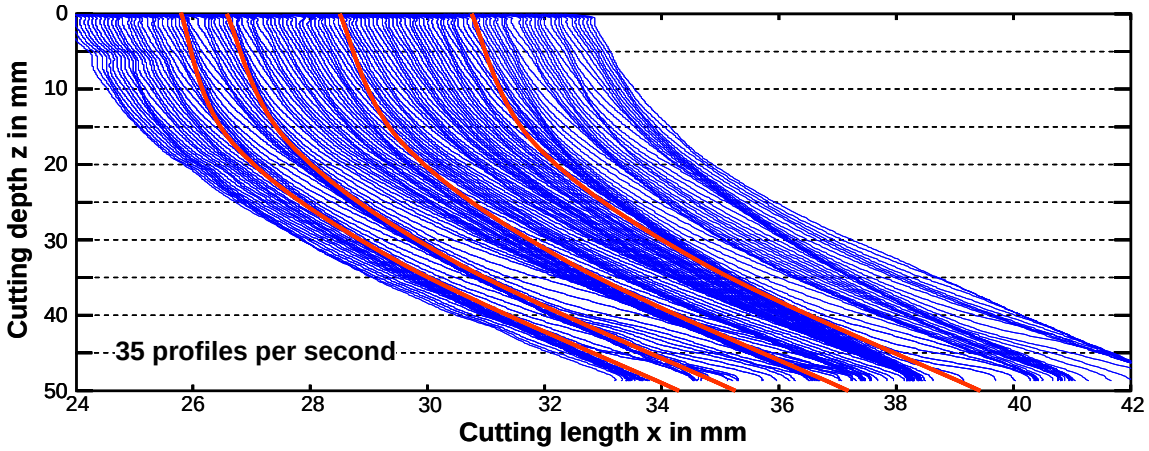

Figure 4: Profiles of the cutting front at 35fps

In Figure 5 a typical time series of cutting front profiles S is displayed with a time-lag of 0,057 seconds between two pictures (17.5fps). The local material removal rate σ(t,z) is displayed at the cutting front. It is calculated from temporal change of the cutting front which is its partial derivative

$$\sigma(t,z) = \partial / \partial t \, S(t,z) \qquad (2)$$

Also the primary contact zone is displayed in the upper area. In the first picture most of the material removal takes place in the upper part, the primary contact zone. The two “hills” of the material removal rate that can be distinguished indicate two different erosion fronts that move

downward (second picture). The upper erosion front moves faster than the lower one, which leads to a coalescence of the two fronts when the faster swallows the slower (picture 3 and 4). In picture 5 the big erosion front moves downwards forming a big step. With this behaviour the major erosion processes can be localized at the steps that were described before. Above the steps as well as below no significant erosion occurs. This behaviour has been predicted by Ditzinger (1999) and Friedrich (2000) in theoretical erosion modeling.

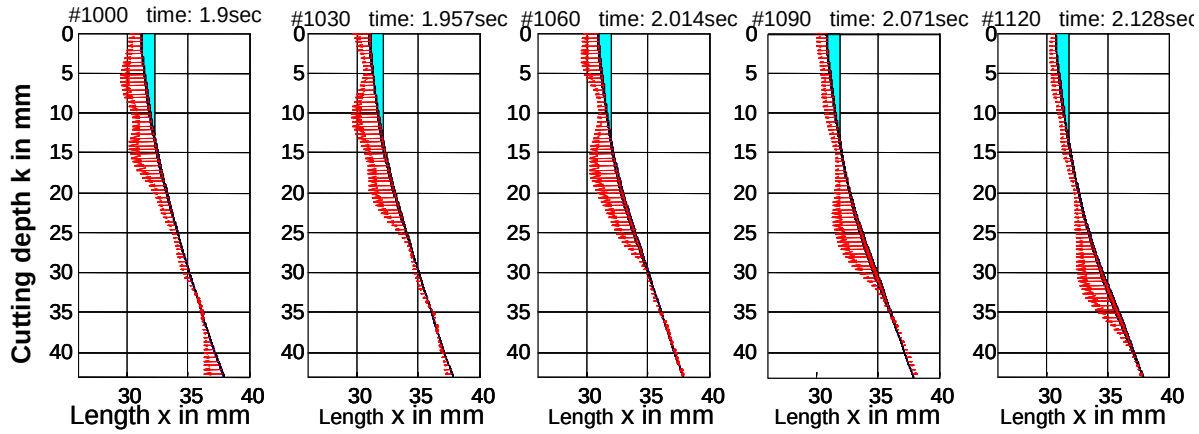

Figure 5: Dynamic behavior of the cutting front with removal rate

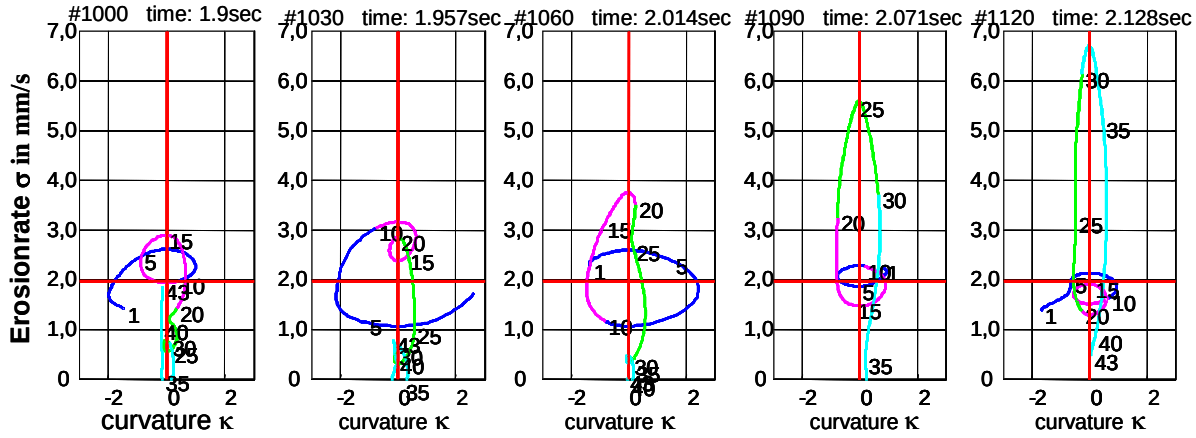

Figure 6: Influence of curvature on erosion rate

The same profiles are shown in Figure 6. Here the material removal rate σ(t,k) is displayed over the local curvature κ(t,k) of the cutting front. The cutting depth is displayed as numbers at the line. The lines show frequent sign-changes of the curvature as can be found in mathematical saddle points (compare Figure 2). This gives strong indication for the existence of steps at the cutting front. At the curvature changes from minus to plus, which would be the top side of the step the material removal rate reaches always its maximum. At the other sign-change it reaches the minimum. With this diagram (Figure 6) the strong correlation between curvature and erosion is proven. In the first picture the curvature starts at negative values (1) with small erosion rates. After the first sign-change the line performs two circles with indicating two small shallow steps.

At the bottom part of the profile only very small curvature with very small erosion occurs. At the second picture the upper erosion front (depth 1-15mm) shows higher absolute curvature values. The lower front (depth 15-20mm) performs a small loop with sharp turns at the step. In the lower part limited erosion occurs. In the third picture the upper front has swallowed the lower forming a new front at a big step with large erosion rates. In fifth picture the erosion front reaches the maximum erosion rates (depth 30mm), while new steps are formed at the top of the profile.

For the understanding of the behaviour of the particle-workpiece interaction at the cutting front needs to be analyzed. The particles flow along the cutting front with multiple shallow angle impacts. The distance between two impacts and its intensity is strongly influenced by the curvature of the cutting front. Still the erosion principle is not as Deam (2004) proposes proportional to the amount of curvature (just like in a meandering river) but rather as can be seen in Figure 6 a result of mulitple impacts of particles forming erosion front at propagate along the cutting front with step formation. The erosion mechanism will be evaluated in the next chapter.

4 MODELLING OF THE EROSION PROCESSES

All erosion effects of particles are due to kinetic impacts. Especially within the primary cutting zone the particles hit the material at very well defined makroskopic geometric conditions. This particle- workpiece interaction can thus be reduced to a very simple situation where a particle with certain properties hits on a surface, causes some effect and eventually leaves the impacting place. In Figure 7 the geometric and kinetic properties are shown. The effect of the impact strongly depends on the parameters like particle velocity v_P, direction θ_P, and rotation ω_P as well as its material properties (e.g. density ρ_P) and its shape. Due to the turbulent character of the process and the diversity of particle sizes and shapes all parameters show a large distribution. Therefore modelling of particle effect and behaviour can only be an averaged qualitative description of the expected behaviour. This still can give valuable information of the relevant processes that take place in the cutting process with abrasive waterjets.

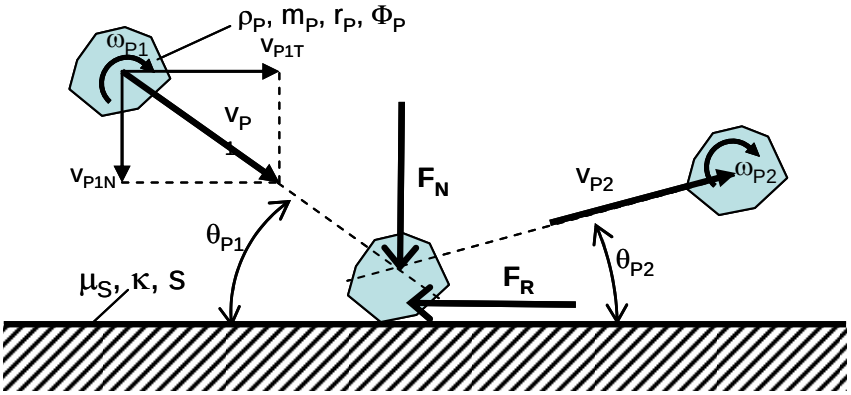

Figure 7: Geometric situation at impact of a particle on a flat surface

4.1 Erosion through direct particle impact

Conventionel model for angle dependent effects of particle impacts are mostly based on the early works of Finnie (1960, 1972) and Bitter (1963). The expected wear at different geometrical conditions was there calculated on the basis of theoretical approaches and experimental verifications. Finnie focuses thereby on the modelling of cutting wear and only corrects his approaches in late publications by introducing microstructured surfaces and rotating particles (Finnie, 1978). This view is supported by the findings of Sheldon (1966), where small particles show ductile wear behaviour also at brittle materials. According to the results of Sheldon (1970, 1972), Goodwin und Tilly (1969), and Tilly (1973) he takes particle properties as rotation, size etc. into account when determining the exponent of the wear function $W_{ges} \propto v_P^n$ to n>2 at different border conditions (Finnie, 1995). Only Deng (2004) experimentally verifies the effect of particle rotatoin and derives a modificated wear model.

Experimental evaluation of plowing impacts (at small impact angles $\theta<\theta_C$) of small particles is subject to relatively large varying geometrical border conditions. Here the very local micrstructure plays an essential role in determining the wear processes. For a plastic deformation prior to material removal a minimal portion of kinetic engery needs to be transferred. According to Bitter (1963) this happens at a specific angle $\sin\tilde{\theta}_P = \tilde{v}_P / v_P$. Hutchings (1979) describes this lower limit by introducing the Best-Number $B = \rho_P \cdot v_P \cdot R_P^{-1}$. Only after reaching a threshold of $B = 10^{-3}$ and suitable particle properties (Wellinger und Uetz, 1979 and Goodwin et. al. ,1969) und Ohlsen (1997) elastic/plastic impacts occur. In abrasive waterjet cutting Blickwedel has taken this into account by introducing a pressure threshold (Blickwedel, 1990).

In abrasive waterjet cutting the dominant wear processes take place at the very cutting front. The particles travel along the cutting front with multiple impacts. While the curvature of the cutting front influences the density of impacts due to the small size of the spheric particles ($r_P<<\kappa^{-1}$) for the very impact the surface can be considered flat and rough (no sliding at the instant of contact). With these assumptions one can determine the kinetic circumstances of a single impact. According to Haug (2002) with this the complex microsopic processes during the impact situation can be analysed with the conservation of momentum theorem.

With this it can be reduced to an excentric impact on a plane surface as shown in Figure 7 . Conservation of momentum $\hat{F}_{x,y}$ leads to

$$\begin{aligned} m_P \cdot (v_{2T} - v_{1T}) &= -\hat{F}_x \\ m_P \cdot (v_{2N} - v_{1N}) &= -\hat{F}_y \\ \Phi_P \cdot (\omega_{P2} - \omega_{P1}) &= -r \cdot \hat{F}_y \end{aligned} \tag{3}$$

With the coefficient of restitution e

$$v_{2N} = e \cdot v_{1N} \tag{4}$$

and the assumption of adhesion in the instant of impact

$$v_{2T} - r_P \cdot \omega_{P2} = 0 \tag{5}$$

With $\Phi_P = \tfrac{2}{5} \cdot m_P \cdot r_P^2$ as section modulus of the sphere one can calculate the exiting velocity of the particle to

$$v_{2T} = \frac{v_{1T} - r_P \cdot \omega_{P1} \cdot \dfrac{\Phi_P}{r_P^2 \cdot m_P}}{1 + \dfrac{\Phi_P}{r_P^2 \cdot m_P}} = \tfrac{5}{7} v_{1T} - \tfrac{2}{7} r_P \cdot \omega_{P1} \tag{6}$$

The rotational speed ω_{P2} is calculated using the tangential exit velocity v_{2T}

$$\omega_{P2} = \frac{-v_{2T}}{r_P} \tag{7}$$

With $v_{1N} = v_1 \cdot \sin\theta_1$ and $v_{1T} = v_1 \cdot \cos\theta_1$ the exit angle θ_2 can be developed to

$$\tan\theta_{P2} = \frac{v_{2N}}{v_{2T}} = \frac{e \cdot v_{1N}}{v_{2T}} = \frac{7 \cdot e \cdot v_1 \cdot \sin\theta_{P1}}{5 \cdot \cos\theta_{P1} \cdot v_1 + 2 \cdot r_P \omega_{P1}} \tag{8}$$

With this the exit angle strongly depends on the coefficient of restitution and the initial rotation of the particle. With higher rotational speed the exit angle decreases. At this assumption no friction occurs. The energy that is transferred from the particle to the surface is

$$W_S = \tfrac{1}{2} m_P \cdot v_1 \cdot \sin\theta_1 \cdot (1 - e) \tag{9}$$

In real impact situations sliding is to be expected. Wear due to sliding only occurs at specific border conditions, though. According to Rumpf (1959) sliding occurs when the kinetic momemtum is larger than stiction. Assuming a straight excentric impact of a small particle on a large workpiece the sliding condition can be stated.

$$\begin{aligned} \hat{F}_X &\geq \mu \cdot \hat{F}_Y \\ m' \cdot v_T \cdot &\geq \mu \cdot m \cdot v_N \\ m_{PR} \cdot (v_P \cdot \cos\theta_P - \omega_{P1} \cdot r_P) &\geq \mu \cdot m \cdot v_P \cdot \sin\theta_P \end{aligned} \tag{10}$$

Taking the rotation of the particle into account the effective impacting angle θ_L is

$$\cot\theta_L = \frac{v_{PT} - \omega_{P1} \cdot r_P}{v_{PN}} \tag{11}$$

Introducing $i^2 = \Phi / m$ and using the reduced particle mass for calculation of the excentric impact. $m_{PR} = m_P \cdot i^2 / \left(i^2 + r_P^2\right)$ and inserting into (10) sliding occurs when the effective impact angle is

$$\cot\theta_L \geq \mu \cdot \frac{i^2 + r_P^2}{i^2} \tag{12}$$

With $\Phi_P = \tfrac{2}{5} \cdot m_P \cdot r_P^2$ for spherical particles and thus $i^2 = \tfrac{2}{5} r_P^2$ this results in

$$\cot\theta_L \geq 7/2\,\mu_S \tag{13}$$

as sliding threshold angle. The transferred friction energy W_{SR} at the impact can therefore be calculated to:

$$W_{SR} = \tfrac{1}{2} m_P \cdot v_P^2 \cdot \sin^2\theta_P \cdot \mu_S \cdot \left(2\cot\theta_L - \mu_S \frac{i^2 + r_P^2}{i^2}\right) \tag{14}$$

According to Rumpf (1959) the total transferred energy does also include deformation energy resulting in

$$W_S = \tfrac{1}{2} m_P \cdot v_P^2 \cdot \sin^2\theta_P \cdot \left(1 + \mu_S \cdot \left(2\cot\theta_L - \mu_S \frac{i^2 + r_P^2}{i^2}\right)\right) \tag{15}$$

With this it is obvious that at low impacting angles the rotational part of the kinetic energy and thus frictions plays the major role in determining the energy transformation. Even without rotation the work due to friction shows interesting behaviour at excentric impacts (Figure 8). Especially at low angle impact conventional systems have problems to describe the effects of erosion. Only when simulating impacts at step like structures the effect can be pictured. With this so far only experimtal generated data could be simulated and the effect of low angle impact could be described. In Figure 8 it can be easily observed that the coefficient of restitution plays a very important role for the erosion behaviour. At low coefficients μ_S=0,1 as it can be found in steel to steel friction the maximum effect can be observed at an impact angle around θ_P=40-50°. At larger coefficients like one would expect at plowing erosion of garnet particles at aluminium with μ_S=0,8 the maximum erosion can be found around θ_P=20°. This simulated behaviour very much complies with experimental wear data.

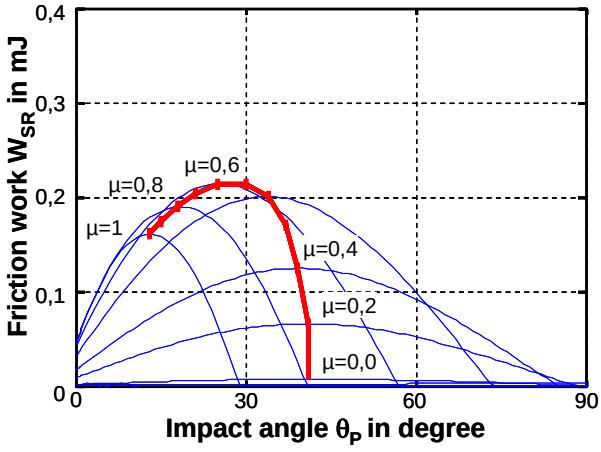

Figure 8: Friction energy at ω_P=0

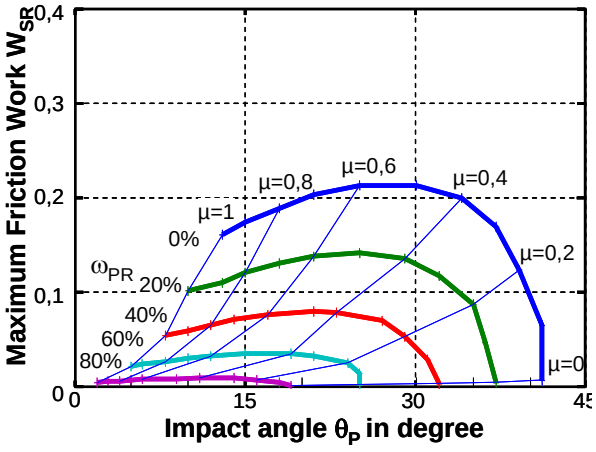

Figure 9: Maximum Friction Work at different coefficients of restitution μ_S and rotations ω_{PR}

As particles travel along the cutting edge with multiple contacts they take on rotational speed up to the point where the circumferential speed equals translatorical velocity. The relative rotational speep ω_{PR} describes the actual part of this maximal speed where only rolling would occur. In Figure 9 the maximum of each curves in Figure 8 is displayed for a selection of friction coefficients and relative rotational speeds. It is very evident that the erosion is significantly reduced with higher rotational speed. Also it is very interesting to see that the most effect of friction occurs at medium values of the friction coefficient.

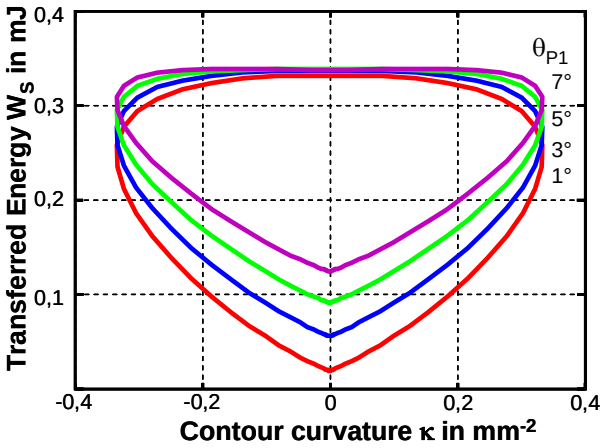

Figure 10:Transferred Energy at variation of entrance angle θ_{P2} at a step (at r_P=90µm, v_0=400m/s)

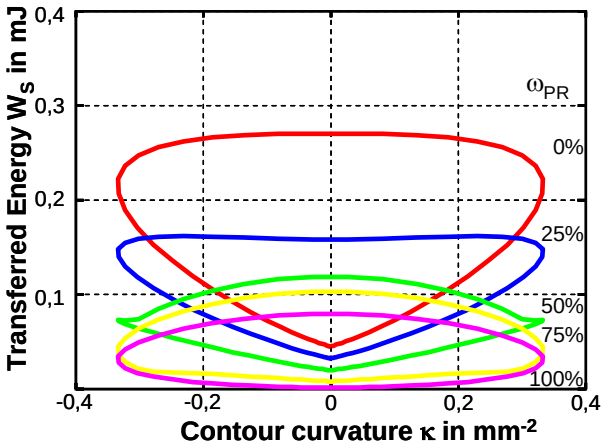

Figure 11: Transferred energy at different rotation ω_{PR} (at r_P=90µm, v_0=400m/s)

4.2 Simulation of impacting behaviour at step formation

In the following simulation of the local erosion behaviour is pictured in more detail. As it was introduced in Figure 2 here the behaviour is analyzed according to the influence of the curvature at the step. Again a closed trajectory can be observed in Figure 10. The shape of the trajectory is a result of the local impact angle and the wear function that is described above. With different entrance angles θ_{P1} the maximal transferred energy does not significantly change. Due to the behaviour of the wear function erosion is stronger at larger impact angles, though. In Figure 11 the effect of rotation of the particles shows not only quantitative but also qualitative changes of the shape of the trajectory. With increasing rotation of the particle the amount of friction wear is significantly reduced. At 100% rotation the rolling condition is fulfilled when the circumferential velocity is equal to the translatorical velocity.

The geometry of the steps can take on different sizes in width and height. In Figure 12 the geometric effects are shown. With increasing height of the step at the same width the local impact angle decreases resulting in lower erosion potential. At small step height the curvature takes on larger values and also larger local impact angles. At very large steps the maximal local impact angle qAmax will exceed the transition angle from plowing to cutting qC as described by Bitter and Finnie. At larger angles of impact the erosion potential decreases most likely resulting in a non uniform erosion pattern as it is shown in Figure 13. The maximum erosion shifts from

the top of the step closer to the limit cycle cutting front resulting in initiation the tertiary cutting zone, which is associated with tunnel boring as it can be found in the rough cutting region.

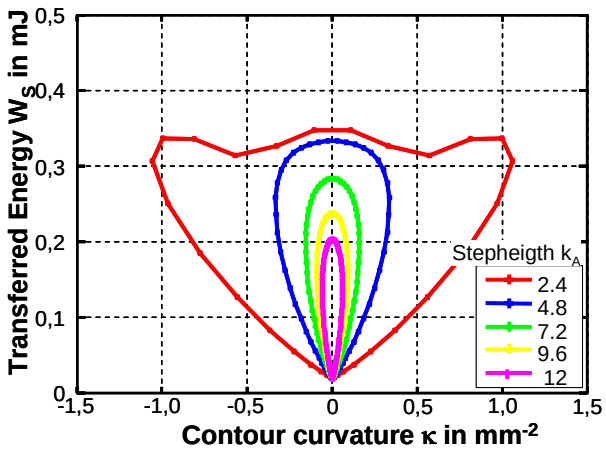

Figure 12: Effect of step geometry on transferred energy at different step heigth k_A (width b_A =1mm)

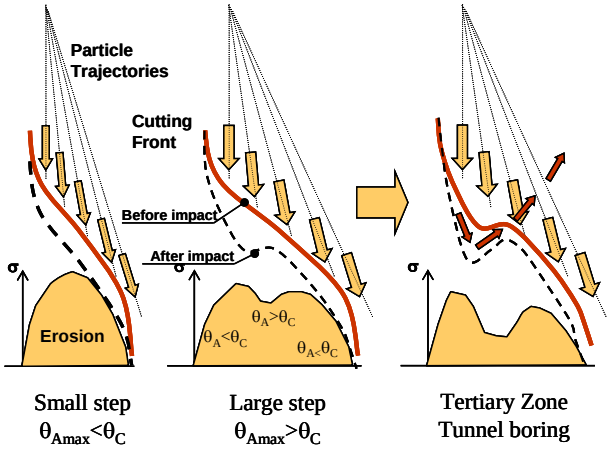

Figure 13: Transition to Tertiary impact zone when large steps occur and maximal $\theta_A>\theta_C$ that leads to tunnel boring

The simulation of the erosion behavior is a new and promising approach to improve the understanding of the very processes that are involved in abrasive waterjet cutting. It was shown that at low angle impact the largest erosion takes place at the very saddle point of the step. Also size and extend of the step like structures play an important role in the erosion behaviour. All the simulation that was performed here took place at very low impact angles where an almost linearly increasing wear behaviour can be observed. As we know from literature the wear function of most metallic materials shows a maximum at a certain impact angle. If this critical angle that was described as the transition from plowing to cutting wear is exceeded at the step formation (this would be most likely at the saddle point) we would expect higher erosion rates before and after that point. This would necessarily lead to a significant change in the geometry of the step resulting in drastic change of erosion behaviour. This point then would most likely then be associated with another point of bifurcation in the cutting process, when in the tertiary phase tunnel boring at the cutting front is initiated.

5 SUMMARY

There have been many approaches to modeling of abrasive waterjet cutting. Despite of high speed camera analysis quantitative evaluation of the spatial- temporal processes at the cutting edge have been hard to acquire. With this approach a high speed geometrical analysis device was utilized to gain detailed information about the geometrical and temporal behaviour of the cutting front. It could be shown that the process always returns to a so called limit cycle where only limited erosion occurs. The most erosion takes place at erosion fronts that travel down the cutting front at a very defined speed. With geometrical analysis it could be shown that the most erosion takes place at the sign change of contour curvature. This leads to the assumption that the erosion mechanism is multiple low angle impacts of particles.

In the second part of this paper the erosion mechanisms were simulated. In a theoretical approach it could be shown that the impacting conditions play the most important role in defining the outcome of the process. At this low angle impact the rotation of the particle and the coefficients of restitution also have a major impact on the erosion process. At this point a new approach towards erosion simulation using step like surfaces was presented. Especially at very low angle impacts it is very likely that surface roughness and wave like micro structures on the surface play a most important role on the evaluation of erosion processes. With this assumption of non regular surfaces new insights towards the effects could be gained. First of all very different erosion behaviour could be simulated just by changing the coefficient of restitution. The other new issue is an approach for the transition point from the secondary impact zone with step formation to the tertiary impact zone which is associated with tunnel boring in the rough cutting region. Here more detailed analysis is necessary to verify and evaluate the findings and to gain more information about how this newly found bifurcation can be influenced.

In this paper new approaches towards analysis of the abrasive waterjet cutting process are presented. For the first time it is now possible to quantitatively analyze the dynamic shape of the cutting front and to gain substantial new insights about the behavior of the cutting process. This can lay the foundation for a new understanding and thus for a better optimization of the process. In order to disseminate the results into in dustrial it must be evaluated, though, how the results can be transferred to a wider range of materials and cutting conditions.

6 REFERENCES

Bitter, J.G.A. (1963) A Study of Erosion Phenomena Part I+II; Wear 6, 5-21, 169-190

Blickwedel, H. (1990) Erzeugung und Wirkung von Hochdruck-Abrasivstrahlen; Fortschrittsberichte VDI - Reihe 2, Nr. 206. Düsseldorf, VDI-Verlag 1990, zugl. Dissertation, Universität Hannover, 1990

Deam, R.T., Lemma, E., Ahmed, D.H. (2004) Modelling of abrasive water jet cutting procespp. WEAR Vol. 257, pp 877-891

Deng, T., Bingley, M.PP., Bradley, M.PP.A, , The influence of particle rotation on the solid particle erosion rate of metals, In: WEAR 256 (2004), Nr. 11-12, pp.1037-1049

Ditzinger, T.; Friedrich, R.; Henning, A.; Radons, G. (1999): Non-Linear Dynamics in Modeling of Cutting Edge Geometry. In: Hashish, Mohamed (Hrsg.); Proceedings of the 10th American Waterjet Conference - Vol. I : August 14-17, 1999, Houston, USA, pp. 15-32

Ditzinger, T.; Friedrich, R.; Henning, A.; Radons, G., Non-Linear Dynamics in Modeling of Cutting Edge Geometry., In: Hashish, M. (Hrsg.): Proceedings of the 10th American Waterjet Conference, 14-17 August 1999, Houston, USA., St. Louis, MO, USA: WJTA, 1999, Vol. 3

Finnie, I. , Erosion of surfaces by solid particle, pp., In: WEAR 3 (1960), Nr. 2, pp. 87-103

Finnie, I. , Some observations on the erosion of ductile metalpp., WEAR 19 (1972), Nr. 1,

Finnie, I. , Some reflections on the past and future of erosion., WEAR 186-187 (1995), Nr. 1 .

Finnie, I. McFadden, A., On the velocity dependence of the erosion of ductile metals by solid particle at low angle incidence., In: WEAR 48 (1978), Nr.1, pp. 181-190

Friedrich, R., Radons, G., Ditzinger, T., Henning, A., Ripple formation through a convective instability from moving and erosion sourcepp. In: Physical review letters 85 (2000) Nr. 23, pp. 4848-4887

Guo, N.PP., Schneidprozess und Schnittqualität beim Wasserabrasivstrahlschneiden., (VDI-Forschritt-Berichte; Reihe 2, Nr. 328), Düsseldorf: VDI-Verlag, 1994, Hannover, Univ., Dis.,1994

Hashish, M. (1988), „Visualization of the abrasive waterjet cutting processes,“ Experimental mechanics 45, 159 (1988), pp. 159-169.

Hauger, W; Schnell, W; Gross, D., Technische Mechanik: Kinetik, Heidelberg: Springer, 2002

Henning, A; Westkämper, E; Analysis of the cutting front in abrasive waterjet cutting. In: Gee,

C. (Hrsg.): Advances and Future Needs. 18th International Conference on Water Jetting, 13-15 September 2006, Gdansk, Poland., Cranfield, Bedford, UK: BHRA, 2006

Henning, A, Westkämper, E. (2003) Modelling of Wear Mechanisms at the Abrasive Waterjet Cutting Front. in: Proceedings of the 2003 WJTA American Waterjet Conference, 3-A

Hutchings, I.M. , Some Comments on the theoretical treatment of erosive particle impacts., In: Field. J. (Hrsg.): Proceedings of the 5th International Conference on Erosion by Solid and Liquid impact. 3-6 September 1979., Cambridge : Cavendish Laboratory, 1979, PP. 1-6.

Hutchings, I.M., Winter, R.E., Field J.E. , Solid Particle Erosion of Metals: The Removal of Surface Material by Spherical Projectilepp., In: Proceedings of the Royal Society of London. Series A, Mathematical and Physical Sciences 348 (1976), Nr. 1654, pp. 379-392

Ohlsen, J. , Recycling von Feststoffen beim Wasserabrasivstrahlverfahren. , (Fortschrittsberichte VDI - Reihe 15, Nr. 175), Düsseldorf: VDI-Verlag, 1997, Hannover, Univ., Diss.,1997

Rumpf, H., Beanspruchungstheorie der Prallzerkleinerung., In: Chemie-Ingenieur-Technik 31 (1959), Nr. 5, pp. 323-337

Sheldon G.L., Kanhere, A. , An investigation of impingement erosion using single particlepp., In: WEAR 21 (1972), Nr.1, pp. 195-209

Sheldon, G.L., Finnie, I. , On the Ductile Behavior of Nominally Brittle Materials During Erosive Cutting., In: Journal of Engineering for Industry 88(1966), pp. 387-392

Sheldon, G.L., Transactions of the ASME., In: Journal on Basic Engineering 92 (1970), pp. 619

Tilly, G P , A two stage mechanism of ductile erosion., In: WEAR 23 (1973), Nr. 1, pp. 87-96

Tilly, G.P. , Erosion caused by airborne particlepp., In: WEAR 14 (1969), Nr.1, pp. 63-79

Zeng, J., Mechanisms of brittle material erosion associated with high-pressure abrasive waterjet processing: A modeling and application study., Kingston, USA, Univ. of Rhode Island, Thesis, 1992.

Zum Gahr, K.H., Microstructure and wear of materials., Amsterdam u.a.: Elsevier, 1987.

7 SYMBOLS

b_A	[mm]	Width of step
d_D	[mm]	Diameter of orifice
d_F	[mm]	Diameter of focussing tube
d_P	[mm]	Diameter of particle
e	[1]	Coefficient of restitution
$\hat{F}_{xyz}$	[kgm/s]	Momentum of particle
F_N , F_T	[N]	Force perpendicular and tangential to surface
F_R	[N]	Friction force
k	[mm]	Cutting depth
m_P	[g]	Mass of particle
R_S	[mm]	Radius of cutting front
S	[mm]	Cutting front
s	[mm]	Arclength of cutting front
$\tilde{v}_P$, $\tilde{\theta}_P$	[mm/min]	Velocity and angle for Bitters model
v_P	[m/s]	Velocity of particle
W_S	[J]	Transferred energy at impact
W_{SR}	[J]	Tranferred friction work at impact
x,y,z	[mm]	Koordinates
Φ_P	[mm^3]	Section modulus of particle
κ	[mm^{-2}]	Curvature of particle
μ_S	[1]	Coefficient of friction
σ	[mm/s]	Material removal rate (σ_M:medium MRR)
θ_A	[°]	Local impact angle
θ_C	[°]	Transition angle from plowing to cutting erosion
θ_P	[°]	Impact angle of particle (before impact θ_{P1}, after impact θ_{P2})
θ_S	[°]	Contour angle of cutting front
θ_L	[°]	Limit angle for friction
ω_P	[s^{-1}]	Rotation of particle (ω_{PR} : part of maximal rotation at impact) (before impact ω_{P1}, after impact ω_{P2})